Electrochimica Acta 56 (2011) 2559–2565

Contents lists available at ScienceDirect

Electrochimica Acta

journal homepage: www.elsevier.com/locate/electacta

Lithium iron phosphate/carbon nanocomposite film cathodes for high energy lithium ion batteries

Yanyi Liu[a], Dawei Liu[a], Qifeng Zhang[a], Danmei Yu[a,b], Jun Liu[c], Guozhong Cao[a,*]

[a] Department of Materials Science and Engineering, University of Washington, Seattle, WA 98195, USA
[b] College of Chemistry and Chemical Engineering, Chongqing University, Chongqing 400044, China
[c] Pacific Northwest National Laboratory, 902 Battelle Boulevard, P.O. Box 999, Richland, WA 99352, USA

ARTICLE INFO

Article history:
Received 16 August 2010
Received in revised form
12 November 2010
Accepted 13 November 2010
Available online 21 November 2010

Keywords:
Lithium-ion battery
Lithium iron phosphate
Intercalation
Surface defect
Nanocomposite

ABSTRACT

This paper reports sol–gel derived nanostructured $LiFePO_4$/carbon nanocomposite film cathodes exhibiting enhanced electrochemical properties and cyclic stabilities. $LiFePO_4$/carbon films were obtained by spreading sol on Pt coated Si wafer followed by ambient drying overnight and annealing/pyrolysis at elevated temperature in nitrogen. Uniform and crack-free $LiFePO_4$/carbon nanocomposite films were readily obtained and showed olivine phase as determined by means of X-Ray Diffractometry. The electrochemical characterization revealed that, at a current density of 200 mA/g (1.2 C), the nanocomposite film cathodes demonstrated an initial lithium-ion intercalation capacity of 312 mAh/g, and 218 mAh/g after 20 cycles, exceeding the theoretical storage capacity of conventional $LiFePO_4$ electrode. Such enhanced Li-ion intercalation performance could be attributed to the nanocomposite structure with fine crystallite size below 20 nm as well as the poor crystallinity which provides a partially open structure allowing easy mass transport and volume change associated with Li-ion intercalation. Moreover the surface defect introduced by carbon nanocoating could also effectively facilitate the charge transfer and phase transitions.

1. Introduction

Recent increases in demand for oil, with the associated environmental sustainable issues are continuing to exert pressure on an already stretched and strained world energy infrastructure. Significant progress has been made in the development of both renewable energy harvesting and storage technologies, such as solar cells, bio-fuels, fuel cells and batteries [1–3]. As one of the most promising clean technology for energy storage, lithium-ion batteries are rapidly gaining the market of batteries, and are attracting significant attention from both research and industry communities, due to its highest energy density and environmentally friendly nature. Due to the fact that the energy storage performance of lithium ion batteries is largely limited by the performance of the cathodic materials, more research has been focused on cathodic materials, such as $LiCoO_2$, $LiMn_2O_4$ and transitional metal oxides [4–6]. Since the first report by Goodenough and his co-workers in 1997 [7] on $LiFePO_4$ applied as cathode materials for lithium ion batteries, it has been attracting much interests both in research and industrial fields because of its high theoretical capacity of 170 mAh/g, flat voltage at ~3.4 V, and good thermal and chemical stability. Moreover it offers economic and environmental advantages being low cost and less toxic material [8,9]. Goodenough and his co-workers showed the possibility of chemically removing lithium from the olivine structure of $LiFePO_4$ thus leaving a new phase $FePO_4$ [7,10–12], with a subtle structural change between $LiFePO_4$ and $FePO_4$ leaving the 1D channels for Li^+-ion motion intact.

Since the limited electronic conductivity of $LiFePO_4$, carbon coating [13,14], metal particles dispersion [15], or aliovalent cations doping [16] have been explored to accelerate the Li^+ diffusion and intercalation. For example, Huang et al. [17] prepared $LiFePO_4$ and conductive carbon nanocomposites with a particle size of 100–200 nm reaching 90% theoretical discharge capacity at a charge rate of C/2, and they concluded that both particle size minimization and intimate carbon contact are necessary for the optimization of electrochemical redox reaction in batteries. Sides et al. [18] used templates to fabricate nanocomposite fibers of $LiFePO_4$–C with the diameter of 350 nm, the unique structure allows a high capacity as 100% of the theoretical value at 3 C, and 36% at a higher discharge rate of 65 C. It was argued that the unique nanostructure improves the lithium ions diffusion in the solid state and the carbon matrix enhances the electronic conductivity [18]. Huang et al. [19] used 7 wt.% of polypyrrole (PPy) as the conductive additives, and electrochemically deposited Carbon coated $LiFePO_4$ (C-LFP)/PPy composite cathodes on stainless steel substrate with a particle size of 2–5 μm. The composite cathodes demonstrated 92% of the capacity charged at 0.1 C when rapidly discharged at 10 C (within 6 min), which was attributed to the good electrical contact

* Corresponding author. Tel.: +1 206 616 9084; fax: +1 206 543 3100.
E-mail address: gzcao@u.washington.edu (G. Cao).

0013-4686/$ – see front matter © 2010 Elsevier Ltd. All rights reserved.
doi:10.1016/j.electacta.2010.11.050

between carbon coated $LiFePO_4$ and PPy, as well as between the particles and the current collector.

In this research, $LiFePO_4$/C nanocomposite film cathodes were fabricated through sol–gel processing followed with annealing and pyrolysis in nitrogen at elevated temperatures. Poor crystallinity, nanostructures together with uniform distribution of carbon on electrochemical performances of these nanocomposite films were characterized and discussed.

2. Experimental

The $LiFePO_4$ sol was prepared from lithium hydroxide monohydrate $LiOH{\cdot}H_2O$ (≥99.0%, Fluka), ferric nitrate $Fe(NO_3)_3{\cdot}9H_2O$ (A.C.S. Reagent, Baker Analyzed) and phosphoric acid H_3PO_4 (A.C.S. Reagent, min. 85%, Spectrum). In order to reduce Fe^{3+} to Fe^{2+} during the preparation and form a complex with the iron ions [15,18], L-ascorbic acid $C_6H_8O_6$ (≥99.0%, Sigma) was added to the solution with the molar ratios of 4:1 to the total metal (Li^+ and Fe^{2+}). Ascorbic acid also plays the role of providing carbon for the $LiFePO_4$/C nanocomposite films after pyrolysis. The overall molar ratio of Li:Fe:P:ascorbic acid was 1:1:1:4. H_3PO_4 and $Fe(NO_3)_3{\cdot}9H_2O$ were first mixed and dissolved in deionized water to form a 1 mol/l solution. $LiOH{\cdot}H_2O$ was then added to the above solution, followed by slowly adding $C_6H_8O_6$ under constant stirring at room temperature. The obtained mixture was stirred at 60 °C for 1 h until the solution turned into dark brownish transparent sol, which was then diluted with more deionized water from 1 mol/l to 0.01 mol/l for the film preparation. It is very crucial to follow the above sequence for the chemical reaction, so that the sol will not become unstable and form precipitations during storage at room temperature.

The $LiFePO_4$/C nanocomposite films were prepared by drop-casting 50 μl of 0.01 mol/l sol onto Pt coated Si wafer and they have a geometric area of approximate 0.2 cm^2. The samples were then dried in ambient conditions overnight and then annealed at various temperatures (500 °C, 600 °C, 700 °C and 800 °C) in N_2 atmosphere for 3 h.

The un-diluted 1 mol/l sol was poured into a petri-dish and dried under ambient conditions for 24 h, and then the residues were collected and ground into fine powders for thermal analysis and X-Ray Diffraction (XRD) measurement. Thermochemical properties of the $LiFePO_4$/C composite powders were investigated by gravimetric analyzer (TGA) and differential thermal analysis (DTA) (PerkinElmer instruments) with the temperature range from room temperature to 800 °C in N_2 atmosphere at a heating rate of 2 °C/min. The XRD (D8 Diffractometer) method was used to detect the phase of the $LiFePO_4$/C composite powders derived from 800 °C. The scanning electron microscopy (SEM) (JEOL JSM-5200) was used to characterize the morphology of $LiFePO_4$/C nanocomposite films after annealed at various temperatures from 500 °C to 800 °C.

Electrochemical properties of the $LiFePO_4$/C nanocomposite films on Pt coated Si wafers were investigated using a standard three-electrode cell setup. 1 mol/l $LiClO_4$ solution in propylene carbonate was used as the electrolyte, a Pt foil as the counter electrode and Ag/AgCl as standard reference electrode respectively. Cyclic voltammetric (CV) and chronopotentiometric measurements (CP) of the $LiFePO_4$/C nanocomposite film cathodes were performed by using an electrochemical analyzer (CH Instruments, Model 605B).

3. Results and discussion

Thermogravimetric analysis (TGA) and differential thermal analysis (DTA) of the $LiFePO_4$/C composite powders which were heated from room temperature to 800 °C at a rate of 2 °C/min in flowing nitrogen is shown in Fig. 1. About 75% weight loss is observed during the temperature sweep to 400 °C, and from 400 °C to 800 °C, the change of weight loss is 5%. The weight loss can be ascribed to the removal of residual solvent, dehydration, decomposition of ascorbic acid and nitrates and possibly the reduction of some remaining Fe^{3+} to Fe^{2+}. It can be observed that the first three endothermic peaks between 81.7 °C and 133.4 °C are due to the removal of residual solvent and dehydration of crystalline water; while the endothermic peak at 392 °C shows the pyrolysis of ascorbic acid from the precursor [20].

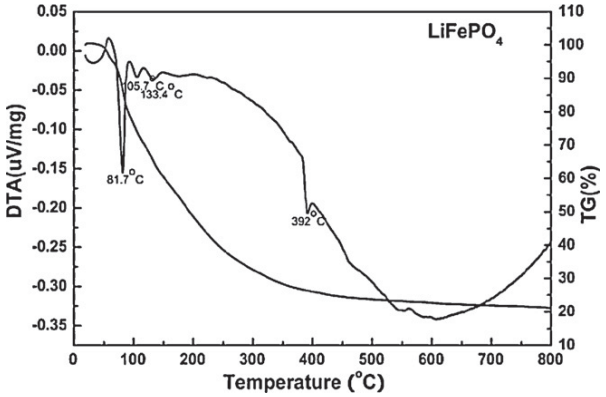

Fig. 1. Thermogravimetric analysis and differential thermal analysis curve of $LiFePO_4$/C composite powders from room temperature to 800 °C at a heating rate of 2 °C/min in nitrogen atmosphere.

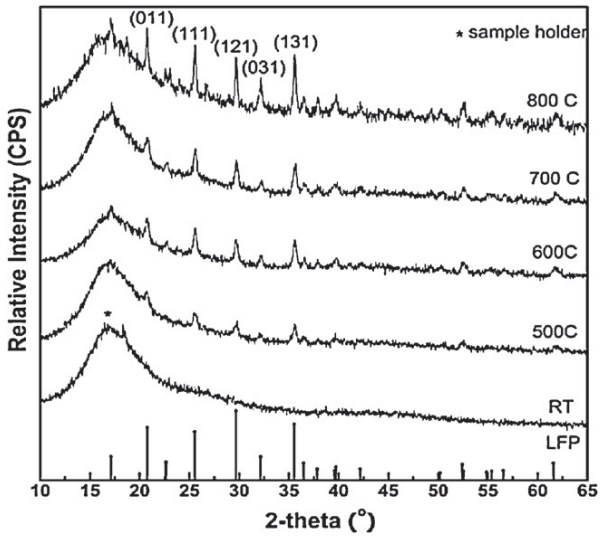

Fig. 2. X-ray diffraction patterns of sol–gel derived $LiFePO_4$/C composite powders at room temperature and heat treated at 500 °C, 600 °C, 700 °C and 800 °C.

Fig. 2 presents XRD patterns of $LiFePO_4$/C composite powders dried from sol at ambient condition, and then annealed at 500 °C, 600 °C, 700 °C and 800 °C, respectively. The powders without annealing showed no detectable peaks, suggesting the amorphous nature. The patterns of powders annealed at 500 °C, 600 °C, 700 °C

Table 1
Crystallite size of $LiFePO_4$/C compsoite powders treated at various temperatures calculated using Scherrer's equation.

Temperature (°C)	Crystallite size (nm)
500	16.1
600	19.4
700	21.1
800	30.8

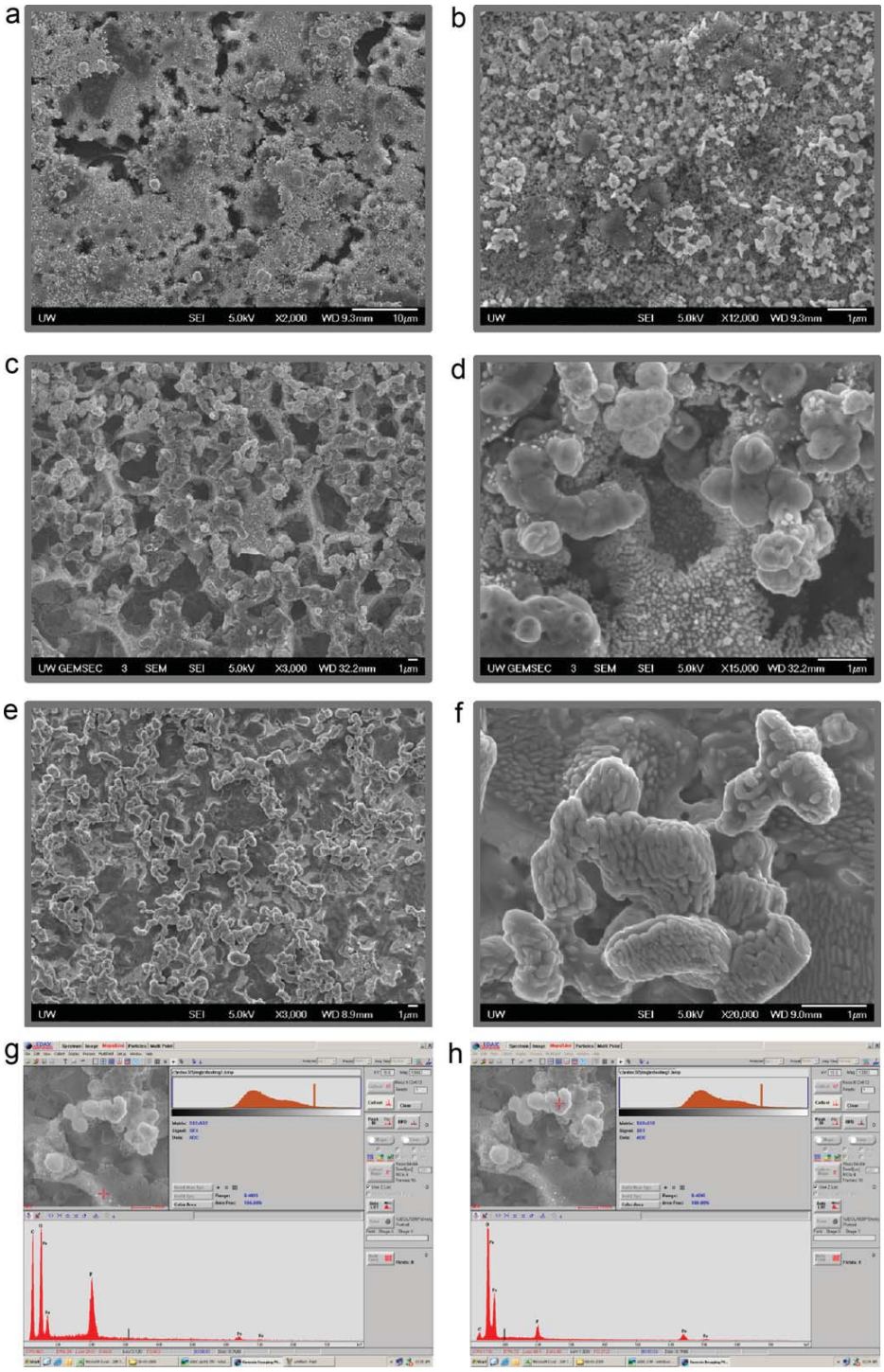

Fig. 3. Scanning Electronic Microscopy (SEM) pictures of $LiFePO_4$/C nanocomposite films annealed at 500 °C (a and b), 600 °C (c and d) and 700 °C(e and f) and Energy-dispersive X-ray Spectroscopy (EDAX) analysis of samples derived from 600 °C (g and h).

and 800 °C clearly showed the evidence of olivine $LiFePO_4$ phase. Among all these XRD patterns, no evidence of diffraction peaks for crystalline carbon (graphite) appeared throughout the temperature range, which indicates that the carbon generated from ascorbic acid is amorphous and its presence does not have detectable influences on the crystal structure of $LiFePO_4$. The comparison of XRD patterns also revealed that, the samples annealed at different temperatures are in the same phase, except that the peaks are gradually sharpened and intensity increases. This suggests an increase in crystallinity, ordering of olivine $LiFePO_4$ phase, growth of grain size as well as release of lattice strain at higher annealing temperature [21].

The crystallite sizes of $LiFePO_4$ in the nano-composite powders treated at different temperatures were calculated using Scherrer's

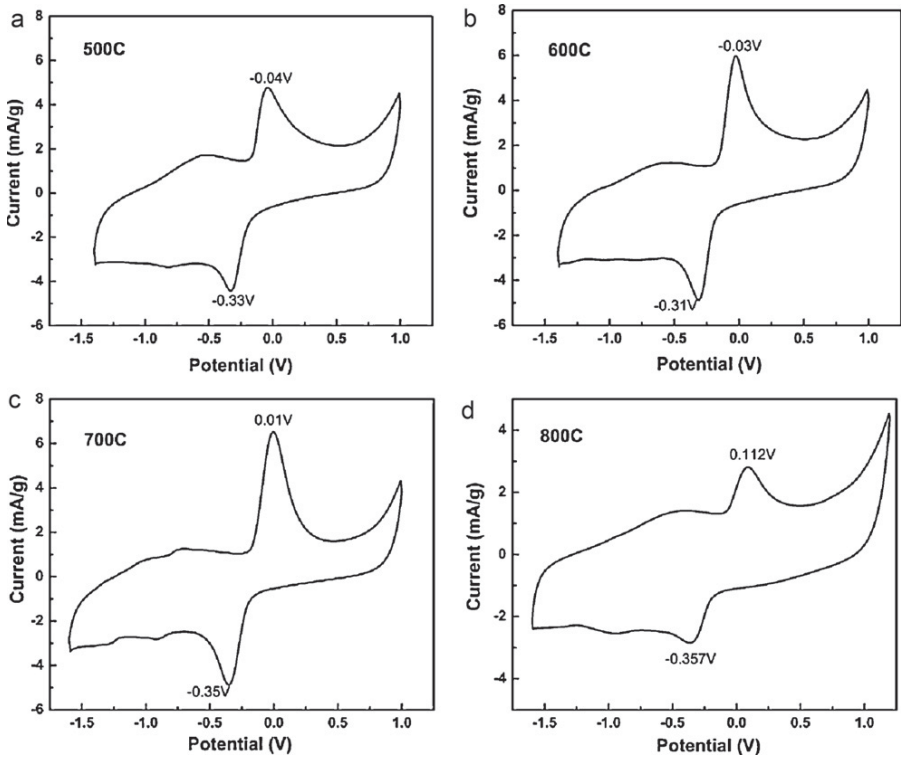

Fig. 4. Traditional electrode composed of active materials, conductive additives and binders (left); sol–gel derived $LiFePO_4$/C nanocomposite cathode films in this study, with $LiFePO_4$ nanocrystallites and carbon nanocoating (right).

equation [22] and the results are shown in Table 1. The crystallite sizes are below or around 20 nm in samples annealed at 500–700 °C, and grow up to 30.8 nm when annealed at 800 °C. The finer $LiFePO_4$ crystallite size compared to the larger crystallite size derived from conventional solid-state synthesis can be ascribed to the sol–gel method applied in this work and the inhibition effect of crystal growth by the presence of carbon nano-coating generated from ascorbic acid intimately mixed in the $LiFePO_4$ sol. This nanostructure with crystallite size under 20 nm could greatly enhance the phase transition during Li-ion intercalation/deintercalation due to the high surface energy, and favored kinetic processes including a short transport pathway and a high and effective contact area with electrolyte [23–25].

Since ascorbic acid was introduced during the sol preparation as a reducing agent of the iron ions [26], upon gelation and pyrolysis at elevated temperatures, the carbon residues are intimately and homogeneously dispersed in the nanocomposites and might be coated onto the $LiFePO_4$ particle surfaces. The thermal annealing effect on the particle size and morphology is evident from the SEM images (Fig. 3(a)–(f)). It can be observed from Fig. 3 that with the increase of annealing temperature from 500 °C to 700 °C, a denser film, and better crystallinity with larger particle size are derived. Fig. 3(a)–(b) are the images under both low and high magnifications of $LiFePO_4$/C nanocomposite films annealed at 500 °C. It can be observed that small particles with loose structures are obtained at 500 °C, and lower crystallinity is derived at this temperature which is in consistent with XRD results. Fig. 3(c)–(d) shows SEM pictures of 600 °C heat treated films, which composes of two distinct phases with different particle sizes. After an energy-dispersive X-ray spectroscopy (EDAX) check of each phase, Fig. 3(g)–(h) show that, small particles are carbon phase while large particles are carbon coated $LiFePO_4$ phase. It can also be seen from Fig. 3(d) that, the carbon particles are homogeneously distributed in the films and some are coated on the surface of $LiFePO_4$ particles, which well guarantees the effective conductive network in the whole film thus improve the electrochemical performance of $LiFePO_4$/C nanocomposite films [26]. The surface carbon could also exist as surface defect which serves as nucleation sites to promote phase transition [6,24]. The three-phase interface of $LiFePO_4$–C–electrolyte could offer a lower nucleation activation energy, therefore the phase transition during Li-ion intercalation/deintercalation is greatly enhanced [27–30]. Further increase the annealing temperature to 700 °C, the morphology of films was examined and shown in Fig. 3(e)–(f). It can be observed that a denser film with better crystallinity and trace of carbon was attained at this temperature. It is also found that both $LiFePO_4$ and carbon particles grow larger and show distinct crystallites morphology when the annealing temperature increases.

A schematic (shown as Fig. 4) demonstrating the distribution and co-existence of carbon with $LiFePO_4$ is proposed based on the XRD, SEM and EDS results discussed above. The carbon residue from ascorbic acid forms an amorphous nano-network in $LiFePO_4$/C nanocomposite films, connecting the individual $LiFePO_4$ particles; the carbon may also wrap around the $LiFePO_4$ particles, and act as both nano-coating to improve the electrical conductivity and surface defect to enhance the lithium ion diffusions. There is also a possibility that porous carbon webs can reside in the interior of the particles, as reported by Chung et al. [31] The conventional electrode process adds 15–20 wt% of conductive additives (carbon black etc.) and binder (PVdF etc.) to the active materials with particles size of micrometer scale, which often gives an inadequate contact between particles thus impedes the lithium ion from diffusing effectively in certain areas. In addition, the additives and binders bring in noticeable mass which further results in a low specific energy and power density counted for the whole electrode. In contrast to the conventional configuration, the carbon network and

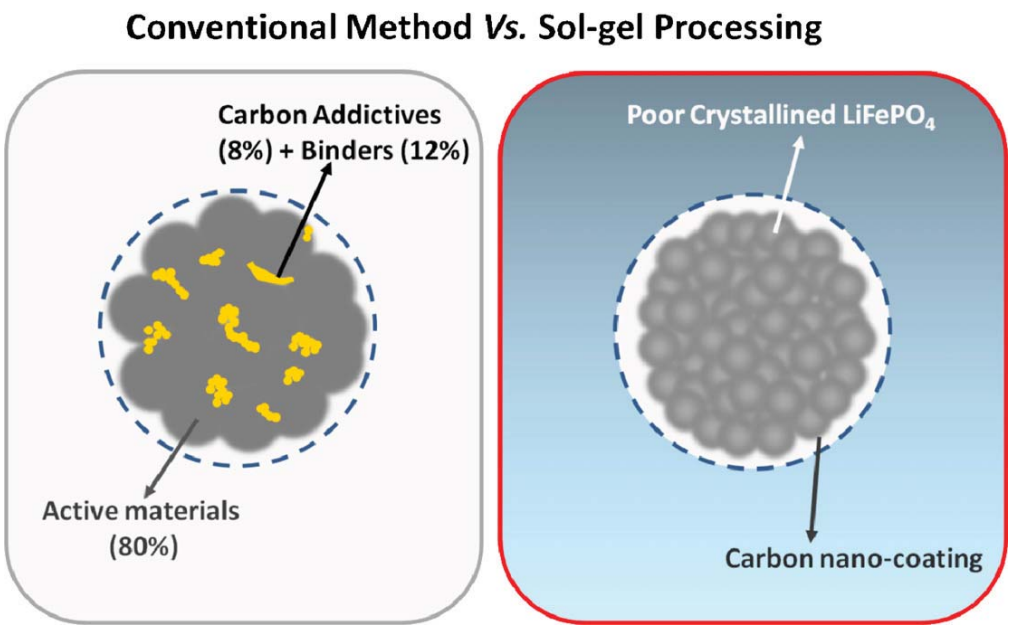

Fig. 5. Cyclic voltammetric (CV) curves of $LiFePO_4$/C nanocomposite films derived from (a) 500 °C, (b) 600 °C, (c) 700 °C, (d) 800 °C (room temperature, 10 mV/s, voltage range: −1.4 V to 1.0 V (*vs.* Ag/Ag^+)).

nanocoating introduced by sol–gel chemistry in this work guarantees a better electrical conductivity, enhanced lithium ion diffusion and higher electrochemical performance as discussed below.

The cyclic voltammetric (CV) curves of $LiFePO_4$/C nanocomposite film cathodes annealed at different temperatures from 500 °C to 800 °C are shown in Fig. 5(a)–(d), which shows distinct redox peaks for intercalation/de-intercalation of lithium ions corresponding to the two-phase charge/discharge reaction of Fe^{2+}/Fe^{3+} redox couple. The anodic oxidation peak for sample that annealed at 500 °C as shown in Fig. 5(a) appears at −0.04 V *vs.* Ag/Ag^+ and cathodic reduction peak at −0.33 V, and the peaks are −0.03 V and −0.31 V for sample that was treated at 600 °C. For the films treated at 700 °C and 800 °C, the CV curves show a wider gap between redox peaks. It was argued by Kim et al. [32] that the smaller gap between redox peaks is more efficient for redox reactions. It is likely that the $LiFePO_4$/C nanocomposite films annealed at 600 °C has more desirable crystallinity as well as nano and micro structure that facilitates redox reactions at the interface and affects the kinetics of transport processes. This result is in consistent with the chronopotentiometric results analyzed in the next paragraphs.

The charge-discharge performances of $LiFePO_4$/C nanocomposite film cathodes derived at different temperatures (500–800 °C) at 200 mA/g are summarized and compared in Fig. 6. The film annealed at 600 °C shows better capacity and cycle stability, as it delivers higher discharge capacity as 312 mAh/g for the initial cycle, and stays 218 mAh/g after 20 cycles. This prominent electrochemical property of $LiFePO_4$/C nanocomposite films treated at 600 °C could be explained by the SEM pictures (Fig. 3(c)–(d)) and XRD results (Fig. 2 and Table 1): the poor crystalline $LiFePO_4$ phase is less compact and more disordering in comparison with well crystallized phase, thus it provides a more flexible structure which could accommodate more lithium ions and facilitate the diffusion within this structure [33]. The $LiFePO_4$ nanocrystallites below 20 nm could also favor the kinetics of phase transition during Li-ion intercalation/deintercalation [34]. Moreover the carbon residing on the surface of $LiFePO_4$ particles could perform as surface defect and buffer material, thereby enhancing the electrochemical capacity and improving cyclic stability [6,34].

For the film annealed at 500 °C, the initial discharge capacity is similarly high as 600 °C sample, which could be ascribed to the amorphous $LiFePO_4$ phase with carbon surface coating that exists in this low temperature treated sample. However a drastic drop of the discharge capacity and poor cyclic performance are detected in this 500 °C film, which shows 139 mAh/g after 13 cycles. This poor cyclic property could be due to the loosely packed microstructure annealed at low temperatures; with increased cycles, the structure may experience irreversible change or loose contact with current collector – similar observations in samples annealed at low temperatures are often found in literature [35,36].

The initial discharge capacities for 700 °C and 800 °C films are 228 mAh/g and 120 mAh/g, which decrease to 148 mAh/g and 99 mAh/g after 20 cycles. The SEM pictures (Fig. 3(e)–(f)) and XRD patterns (Fig. 2) show that more compact and well crystallized structures are obtained in higher temperature annealed films, which gives less freedom and open space for lithium ion diffusion,

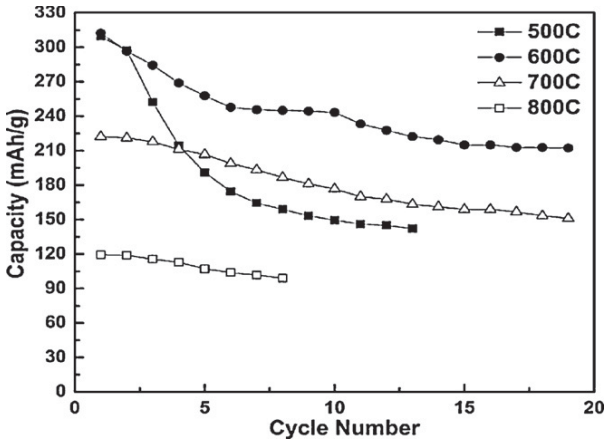

Fig. 6. Discharge capacities of sol–gel derived $LiFePO_4$/c nanocomposite cathode films annealed at 500–800 °C at a discharge rate of 200 mA/g.

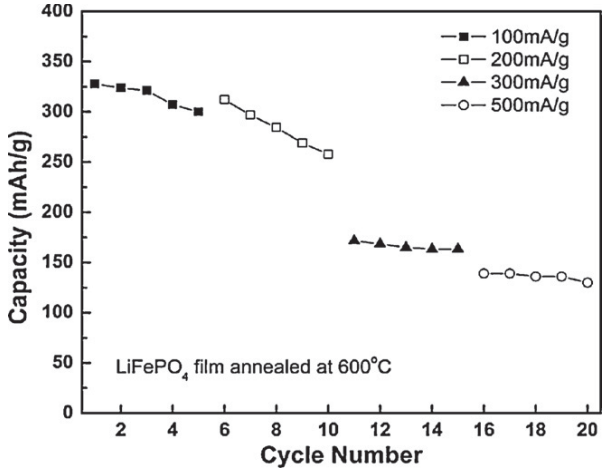

Fig. 7. Lithium ion intercalation capacities of sol–gel derived $LiFePO_4$/C nanocomposite cathode films annealed at 600 °C as a function of cycles under different discharge rates.

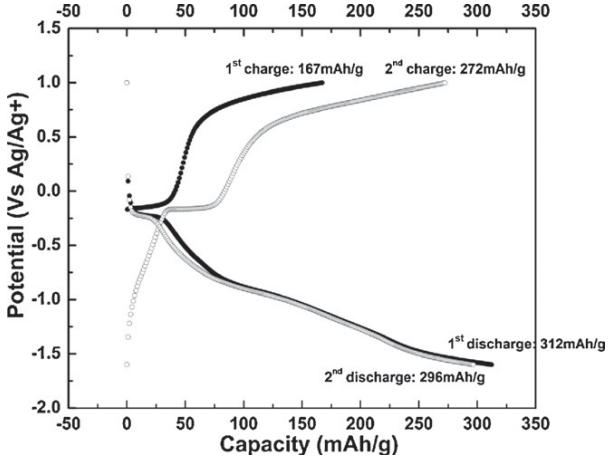

Fig. 8. The first and second charge/discharge curves of sol–gel derived $LiFePO_4$/C nanocomposite cathode films annealed at 600 °C at a discharge rate of 200 mA/g.

thus lower discharge capacities are measured from this research. The poorer electrochemical performances at higher annealing temperatures could also be ascribed to the enlarged particle size with the increase of temperature. Since charge transfer resistance is related to the difference of particle size. A decrease in particle size will decrease the polarization associated with electronic and/or ionic resistance, thus improve the reversible capacity. The larger particles present as transport limitation both for lithium ions and electron diffusion, which results in capacity loss [37].

The charge-discharge performance at different charging rate of $LiFePO_4$/C nanocomposite film cathodes annealed at 600 °C is shown in Fig. 7. In this experiment, we conducted the intercalation and deintercalation at the same rate for a specific sample and all samples were measured between −1.6 V and 1.0 V (Vs Ag/Ag^+). The as-prepared $LiFePO_4$/C nanocomposite film cathodes demonstrate a high initial specific discharge capacity of 327 mAh/g at the current density of 100 mA/g (0.6 C). When the current density is 200 mA/g (1.2 C), the initial capacity is 312 mAh/g, and the initial capacities show 171 mAh/g and 139 mAh/g at higher rate of 300 mA/g (1.8 C) and 500 mA/g (3 C) respectively. This high discharge capacity at a high rate could be ascribed to the surface defect and enhanced electronic conductivity due to the carbon nano-coating at the $LiFePO_4$ particle surface [6,29]. This carbon coating can well provide a better connecting network for electron diffusion [35]. Moreover the shortened transportation path as well as the enhanced phase transition kinetics of lithium ion intercalation/de-intercalation could be ascribed to the nanoscaled structure [36,38,39].

The sol–gel derived $LiFePO_4$/C nanocomposite film cathodes demonstrated a discharge capacity of over 300 mAh/g, exceeding the theoretical value of 170 mAh/g reported in literature [40]. Fig. 8 presents the first charge and discharge curve at a rate of 200 mA/g, and it could be observed that the charge capacity of the first cycle is 167 mAh/g, which almost equals theoretical value of well crystallized bulk $LiFePO_4$, indicating that the initial sol–gel derived $LiFePO_4$/C nanocomposite films consist of stoichiometric chemical composition with an atomic ratio of Li^+:Fe^{2+}:$PO_4{}^{3+}$ = 1:1:1 as it was designed in the sol processing and sample preparation. This result is in good agreement with the XRD patterns as shown in Fig. 2, and it also validates that during the first charge step, all the Li^+ ions extracted from the $LiFePO_4$/C nanocomposite films, as was measured to be 168 mAh/g in capacity. However at the subsequent discharge process, a capacity of 312 mAh/g was measured, which shows that the amount of Li ions that intercalate into the film exceeds the theoretical value for a stoichiometric crystalline $LiFePO_4$. Although there is a gradual degradation of the electrochemical performances with increase cycles, the capacity of $LiFePO_4$/C nanocomposite films stays above the theoretical limit within the number of cycles conducted in this study. The lack of well-defined plateau for the discharge curve in Fig. 8 in comparison with other work on $LiFePO_4$ [16–19,23,24] could also be an indication of the poor crystallinity at high discharge rate of 1.2 C. This experimental result has shown its reproducibility and all the measurements conditions are carefully verified.

The exact explanation for such a high lithium ion intercalation capacity is not known and a number of experiments are underway to get insights for a fundamental understanding, however, capacities higher than theoretical limit observed in other nanostructured electrode materials have also been reported in literatures by other authors [40–44]. For example, O'Dwayer et al. [40] observed that the VOTPP-based VO_x nanotubes exhibited remarkable charge capacities of 437 mAh/g, which exceeds the reported theoretical value of 240 mAh/g [45], and they believe that it is the increased volumetric density of nanotubes for ion intercalation and shorter diffusion paths which provide better freedom for dimensional change that occurs during intercalation and deintercalation reactions. Wang et al. [41] fabricated TiO_2-graphne hybrid nanostructured materials and tested them as anode materials for Li-ion batteries. They observed high Li-ion intercalation capacities of ∼200 mAh/g at C/5 for rutile TiO_2–0.5 wt% graphene, and ∼200 mAh/g at 1 C for rutile TiO_2–10 wt% graphene hybrid materials during the first 10 cycles, which exceeds the theoretical capacity of 168 mAh/g for bulk rutile TiO_2 materials. They believed that the high intercalation properties and enhanced kinetics in TiO_2–graphene hybrid materials can be attributed to the improved conductivity with the incorporation of highly conducting graphene, and this self-assembled hybrid materials are more effective compared with the conventional electrodes fabricated with conductive additives and binders. Jiang et al. [42] observed high Li-ion storage capability, high rate performance and cyclability in nanometer-sized rutile TiO_2 electrode, with ∼378 mAh/g of Li-ion intercalation capacity for the initial cycle, which is corresponding to more than 1 Li^+ being inserted into TiO_2. For rutile TiO_2, Li-ion diffusion occurs mainly through *c* channels and the sluggish Li diffusion in the *a*–*b* planes is the bottleneck for further Li-ion insertion. [46] Jiang et al. believed that the limit of Li-ion diffusion in *a*–*b* planes was weakened in nanometer-sized rutile TiO_2, which means that more thermodynamically stable

octahedral sites in *a*–*b* planes can be reached by Li ions, providing more pronounced intercalation sites for Li-ions. Liu et al. [43] reported that the mesoporous hydrous manganese dioxide nanowall arrays achieved a stable high intercalation capacity of 256 mAh/g, exceeding the theoretical limit of 150 mAh/g for manganese dioxide bulk film. They argued that such high capacity is ascribed to the hierarchically structured macro- and mesoporosity of $MnO_2{\cdot}0.5H_2O$ nanowall arrays, which provides a large surface to volume ratio favoring interface Faradaic reactions, short solid-state diffusion paths, and freedom to permit volume change during lithium ion intercalation and de-intercalation. Based on quantum theory, Raebiger et al. [47] proposed that there is no noticeable net charge change of the oxidation state of a transition metal in a crystal lattice changes associated with lithium ion intercalation, and instead the intercalation is due to the change of hybridization as a result of the change of its energy level relative to the surrounding atoms (e.g. oxygen in transition metal oxides). Therefore the irrelevant relationship between static charges of transition metal and its oxidation status change upon removal or addition of electrons could bring a re-examination of the theoretical capacity value to electrode materials for lithium ion batteries. The excellent performance of the sol–gel derived $LiFePO_4$/C nanocomposite cathode films observed in this study may be attributed to the relatively poor crystallinity of $LiFePO_4$ nanocrystallites offering more available sites for Li-ion intercalations, as well as the intimate contact of carbon to $LiFePO_4$ crystallites, serving as both surface defects and electronic conductive coatings and networks, which effectively enhances the conductivity of composite film electrodes. This unique nanocomposite structure could result in an enhanced electrochemical performance with much improved transport properties and storage capacity through facilitating the phase transition during Li-ion intercalation/deintercalation processes.

4. Conclusions

$LiFePO_4$/carbon nanocomposite film cathodes are readily fabricated by sol–gel processing with excessive polymer additive followed with annealing and pyrolysis in an inert gas at elevated temperatures for lithium ion batteries, with carbon serving as both defects and conductive nanocoating on the surface of $LiFePO_4$ particles. Crystal, nano and microstructure of the $LiFePO_4$/C nanocomposite films can be tuned through controlling the subsequent annealing process. High electrochemical performance with initial discharge capacity of 312 mAh/g and good cyclic stability (218 mAh/g after 20 cycles) were observed for $LiFePO_4$/C nanocomposite film cathodes annealed at 600 °C when tested within 1.0 V to −1.6 V (*vs.* Ag^+/Ag). The exceptionally high electrochemical performances could be ascribed to the $LiFePO_4$ nanocrystallites with large surface to volume ratio and possible surface defects, and the relatively poor crystallinity which provides a less packed structure to accommodate more lithium ions. Furthermore, the carbon surface defects and conductive nanocoating may effectively improve the charge-transfer property and phase transition during Li-ion intercalation/deintercalation.

Acknowledgements

This research work has been financially supported by Nation Science Foundation (DMR-0605159 and CMMI-#1030048), Air Force Office of Scientific Research (AFOSR-MURI, FA9550-06-1-0326), and Pacific Northwest National Laboratory (PNNL).

References

[1] P.D. Lund, Renewable Energy 32 (2007) 442.
[2] W. Hoffmann, Solar Energy Mater. Solar Cells 90 (2006) 3285.
[3] Q.F. Zhang, T.P. Chou, B. Russo, S.A. Jenekhe, G.Z. Cao, Angew. Chem. Inter. Ed. 47 (2008) 2402.
[4] P.N. Kumta, D. Gallet, A. Waghray, G.E. Blomgren, M.P. Setter, J. Power Sources 72 (1998) 91.
[5] M.M. Thackeray, J. Electrochem. Soc. 142 (1995) 2558.
[6] D.W. Liu, Y.H. Zhang, P. Xiao, B.B. Garcia, Q.F. Zhang, X.Y. Zhou, Y.-H. Jeong, G.Z. Cao, Electrochim. Acta 54 (2009) 6816.
[7] A.K. Padhi, K.S. Nanjundaswamy, J.B. Goodenough, J. Electrochem. Soc. 144 (1997) 1188.
[8] V. Srinivasan, J. Newman, Electrochem. Solid-State Lett. 9 (2001) A110.
[9] N. Meethong, H.Y.S. Huang, W.C. Carter, Y.-M. Chiang, Electrochem. Solid-State Lett. 10 (2007) A134.
[10] A.K. Padhi, K.S. Nanjundaswamy, C. Masquelier, S. Okada, J.B. Goodenough, J. Electrochem. Soc. 144 (1997) 1609.
[11] J.B. Goodenough, J. Power Sources 174 (2007) 996.
[12] G. Chen, X. Song, Electrochem, Solid State Lett. 9 (2006) A295.
[13] Y. Wang, Y. Wang, E. Hosono, K. Wang, H. Zhou, Angew. Chem. Int. Ed. 47 (2008) 7461.
[14] J.-K. Kim, G. Cheruvally, J.-H. Ahn, J. Solid State Electrochem. 12 (2008) 799.
[15] F. Croce, A.D. Epifanio, J. Hassoun, A. Deptula, T. Olczac, B. Scrosati, Electrochem. Solid-State Lett. 5 (2002) A47.
[16] S.-Y. Chung, J.T. Bloking, Y.-M. Chiang, Nat. Mater. 1 (2002) 122.
[17] H. Huang, S.-C. Yin, L.F. Nazar, Electrochem. Solid-State Lett. 4 (2001) A170.
[18] C.R. Slides, F. Croce, V.Y. Young, C.R. Martin, B. Scrosati, Electrochem. Solid-State Lett. 8 (2005) A484.
[19] Y.-H. Huang, J.B. Goodenough, Chem. Mater. 20 (2008) 7237.
[20] S.-Q. Liu, S.-C. Li, Chin. J. Inorg. Chem. 22 (2006) 645.
[21] G.H. Li, H. Azuma, J. Electrochem. Soc. 149 (2002) A743.
[22] R. Jenkins, R.L. Snyder, Introduction to X-ray Powder Diffractometry, John Wiley & Sons Inc., 1996, P89.
[23] C. Delacourt, P. Poizot, S. Levasseur, C. Masquelier, Electrochem. Solid-State Lett. 9 (2006) A352.
[24] X. Yan, G. Yang, J. Liu, Y. Ge, H. Xie, X. Pan, R. Wang, Electrochim. Acta 54 (2009) 5770.
[25] D.J. Reidy, J.D. Holmes, M.A. Morris, J. Eur. Ceram. Soc. 26 (2006) 1527.
[26] J.D. Wilcox, M.M. Doeff, J. Electrochem. Soc. 154 (2007) A389.
[27] X.H. Wang, J.-G. Li, H. Kamiyama, M. Katada, N. Ohashi, Y. Moriyoshi, T. Ishigaki, J. Am. Chem. Soc. 127 (2005) 10982.
[28] H. Liu, W. Yang, Y. Ma, Y. Cao, J. Yao, New J. Chem. 26 (2002) 975.
[29] D.W. Liu, Y.Y. Liu, B.B. Garcia, Q.F. Zhang, A.Q. Pan, Y.-H. Jeong, G.Z. Cao, J. Mater. Chem. 19 (2009) 8789.
[30] M.M. Doeff, J.D. Wilcox, R. Yu, A. Aumentado, M. Marcinek, R. Kostecki, J. Solid State Electrochem. 12 (2008) 995.
[31] H.-T. Chung, S.-K. Jang, H.W. Ryu, K.-B. Shim, Solid State Commun. 131 (2004) 549.
[32] J.-K. Kim, J.-W. Choi, G.S. Chauhan, J.-H. Ahn, G.-C. Hwang, J.-B. Choi, H.-J. Ahn, Electrochim. Acta 53 (2008) 8258.
[33] P. Jozwiak, J.E. Garbarczyk, M. Wasiucionek, I. Gorzkowska, F. Gendron, A. Mauger, C. Julien, Mater. Sci.: Poland 27 (2009) 307.
[34] J. Liu, G.Z. Cao, Z.G. Yang, D.H. Wang, D. Dubois, X. Zhou, G.L. Graff, L.R. Pederson, J.-G. Zhang, ChemSusChem 1 (2008) 676.
[35] A.D. Spong, G. Vitins, J.R. Owen, J. Electrochem. Soc. 152 (2005) A2376.
[36] Z.C. Shi, A. Attia, W.L. Ye, Q. Wang, Y.X. Li, Y. Yang, Electrochim. Acta 53 (2008) 2665.
[37] Z. Xu, L. Xu, Q. Lai, X. Ji, Mater. Chem. Phys. 105 (2007) 80.
[38] J. Maier, Nat. Mater. 4 (2005) 805.
[39] A.S. Arico, P. Bruce, B. Scrosati, J.M. Tarascon, W. Van Schalkwijk, Nat. Mater. 4 (2005) 366.
[40] C. O'Dwyer, V. Lavayen, D.A. Tanner, S.B. Newcomb, E. Benavente, G. Gonzalez, C.M. Sotomayor Torres, Adv. Funct. Mater. 19 (2009) 1736.
[41] D.H. Wang, D.W. Choi, J. Li, Z.G. Yang, Z.M. Nie, R. Kou, D.H. Hu, C.M. Wang, L.V. Saraf, J.G. Zhang, I.A. Aksay, J. Liu, ACS NANO 3 (2009) 907.
[42] C.H. Jiang, I. Honma, T. Kudo, H.S. Zhou, Electrochem. Solid-State Lett. 10 (2007) A127.
[43] D.W. Liu, B.B. Garcia, Q.F. Zhang, Q. Guo, Y.H. Zhang, S. Sepehri, G.Z. Cao, Adv. Funct. Mater. 19 (2009) 1015.
[44] Y. Wang, G.Z. Cao, Adv. Mater. 20 (2008) 2251.
[45] S. Nordlinder, J. Lindgren, J. Electrochem. Soc. 150 (2003) E280.
[46] A. Stashans, S. Lunell, R. Bergstrom, Phys. Rev. B 53 (1996) 159.
[47] H. Raebiger, S. Lany, A. Zunger, Nature 453 (2008) 763.